Two Transport Pathways for Fetuin-A-based Mineral Complexes in Osteogenic Matrix Mineralization

Authors: Judith M. Schaart[1], Luco Rutten[1,2], Shaina V. To[1,2], Alisha A. Shah[1], Martijn Martens[1,2], Elena Macías-Sánchez[1,2,3], Willi Jahnen-Dechent[4], Nico Sommerdijk[1,2]*, Anat Akiva[1,2]*

Affiliations:
[1] Department of Medical BioSciences, Radboud University Medical Center; Nijmegen, The Netherlands.
[2] Electron Microscopy Center, Radboudumc Technology Center Microscopy, Radboud University Medical Center; Nijmegen, The Netherlands.
[3] Department of Cell Biology and Immunology, Institute of Parasitology and Biomedicine "López-Neyra", Spanish National Research Council (CSIC), 18016 Granada (Spain).
[4] Helmholtz Institute for Biomedical Engineering, Biointerface Laboratory, RWTH Aachen University Hospital; Aachen, Germany.

* Corresponding author. Email: anat.akiva@radboudumc.nl; nico.sommerdijk@radboudumc.nl

Abstract:
Mineral transport in vertebrates poses a paradox: calcium and phosphate must circulate safely in soluble form, yet be delivered in massive quantities to bone. The liver-produced circulating protein Fetuin-A forms protein-mineral complexes that prevent soft tissue calcification, but its high abundance in bone also suggests a role in matrix mineralization. We show that Fetuin-A supports two mineral trafficking pathways: small complexes enable direct delivery, while larger calciprotein particles (CPPs) are endocytosed by osteoblasts before contributing to mineralization. We propose that the CPP pathway is activated during high systemic demand, such as fetal development. Using cryogenic and liquid-phase electron microscopy, combined with cell models, we propose Fetuin-A as a regulator of systemic mineral balance, integrating liver, blood, and bone physiology in a unified mineral transport system.

Main text:

Introduction

Living organisms face a fundamental challenge in mineral transport: ions such as calcium and phosphate must circulate at high concentrations in blood, yet remain soluble to avoid pathological calcification. At the same time, these same ions must be delivered in bulk to support skeletal development and continuous bone remodeling. Yet, it remains poorly understood how vertebrates solve this paradox - stabilizing mineral during transport while enabling its controlled deposition into bone.

Fetuin-A (FetA), also known as α_2-Heremans Schmidt Glycoprotein, has emerged as a key player in mineral metabolism. It is a liver-produced glycoprotein that is secreted into the blood where it binds calcium phosphate (CaP) to form soluble protein-mineral complexes that prevent mineral precipation and protect soft tissues such as the kidney and blood vessels from ectopic calcification. (*1-3*) Indeed, dysregulation of Fetuin-A complexes is strongly implicated in chronic kidney disease and vascular pathology. (*4-7*) Yet paradoxically, Fetuin-A is also one of the most abundant non-collagenous proteins in bone, (*8, 9*) suggesting that beyond its protective role in circulation, it contributes directly to skeletal mineralization.

Protein–mineral complexes formed with Fetuin-A exist in multiple states. Small, soluble complexes, called calciprotein monomers (CPMs), are thought to carry pre-nucleation mineral clusters, while larger calciprotein particles (CPPs) contain amorphous (primary CPP, Ø50-100 nm) or crystalline (secondary CPP, Ø100-500 nm) calcium phosphate. (*1, 8, 10*) These species are dynamic, with their size and composition reflecting systemic conditions such as mineral load, protein concentration, and metabolic state.ref Despite their clear relevance to physiology and disease, the precise roles of Fetuin-A-based protein-mineral complexes in delivering mineral to the extracellular bone matrix have not been defined.

Here, we combine cryogenic and liquid-phase electron microscopy with biochemical assays and osteoblast cultures to unravel the formation mechanism of primary CPPs and shed light on the mechanisms of Fetuin-A-mediated mineral transport. We show that two fundamentally distinct pathways operate in parallel. Small complexes directly deposit mineral into collagen fibrils, sustaining the steady turnover of bone during homeostatic processes such as bone remodeling. In contrast, larger aggregates require cellular uptake and lysosomal processing by osteoblasts before their mineral becomes available for matrix deposition. It is conceivable that this indirect, transcellular pathway is upregulated when systemic mineral demand is high, such as during fetal development, when circulating concentrations of Fetuin-A and calcium phosphate peak. (*11, 12*)

Results

Formation of Fetuin-A–based protein–mineral complexes

To generate biomimetic Fetuin-A–mineral complexes in the high phosphate physiological protein milieu in which calciprotein complexes form, we increased the phosphate concentration (4.75 mM, Fig. S1A) of serum-containing cell culture medium at 37 °C. (*7*) Dynamic light scattering revealed a rapid increase in particle size between 10 and 30 minutes, stabilizing at ~100 nm, consistent with the complete transition from soluble CPMs to particulate CPPs (Fig. 1A). CryoTEM imaging showed virtually no CPMs but only spherical CPPs ranging from 20 to 100 nm in diameter (Fig. 1B, Fig. S2/S3) and protein from the medium. CPPs and medium proteins were differentiated on the bases of their contrast in the cryoTEM images (Fig. S2/S3). Selected-area electron diffraction showed diffuse scattering rings characteristic of amorphous calcium phosphate, confirming they were primary CPPs (Fig. 1C). High-resolution images revealed that individual CPPs consisted of 2–5 nm subunits, likely representing aggregated CPMs (Fig. 1B$_i$). We note that although FetA has been reported as the main protein supporting CPP formation, the contribution of other serum proteins, e.g albumin, cannot be ruled out. (*13*)

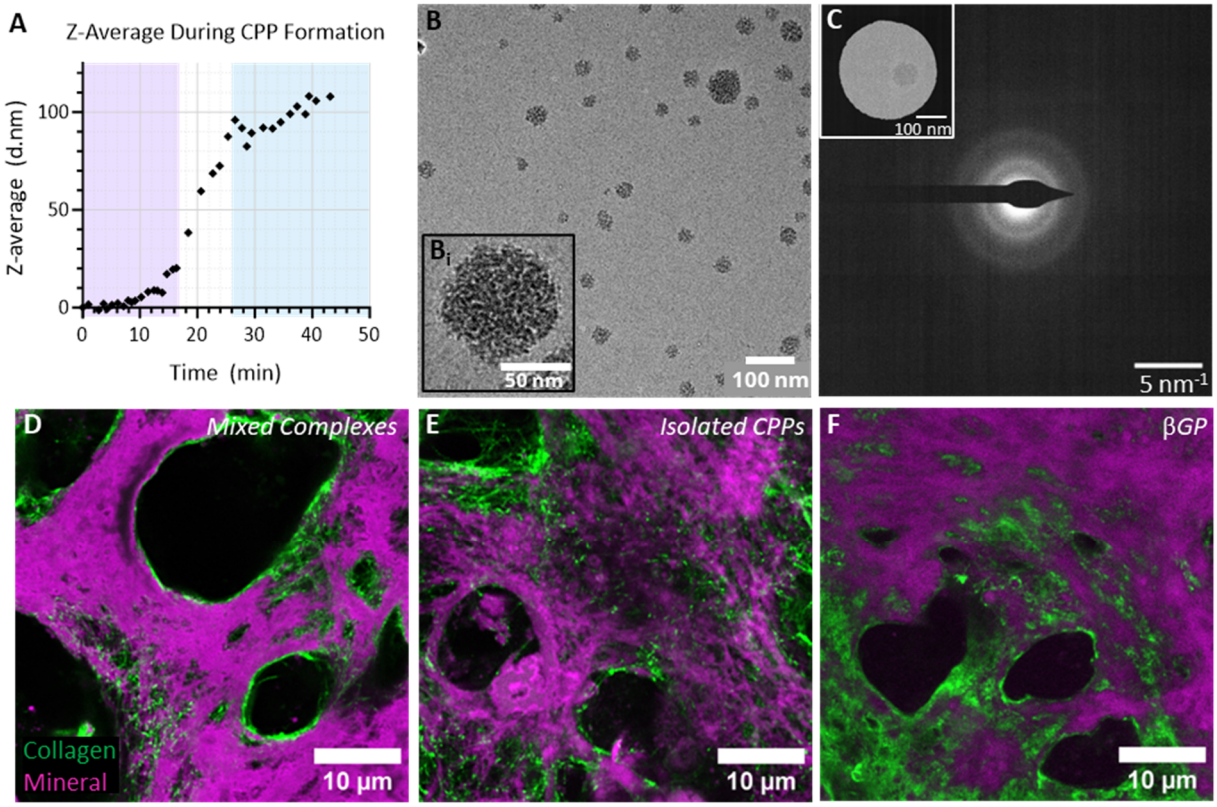

Fig. 1. CPP Formation and Mineralization Capacity in Osteoblast Cultures (**A**) Time-resolved DLS shows a stable Z-average (close to 0 nm after background correction) in the first 16 minutes after addition of phosphate to complete cell culture medium (magenta). Next, the measured Z-average largely increases (white), after which a new size equilibrium (~105 nm) is reached around 25 minutes after the start of the reaction (blue). (**B**) CryoTEM shows the presence of spherical complexes with diameters ranging from 20 to 100 nm in complete cell culture medium supplemented with phosphate after 24h of incubation. (**Bi**) The particles are composed of multiple smaller particles, as observed with high-resolution imaging. (**C**) Low dose selected area electron diffraction confirms that the formed CPPs contain amorphous mineral. **D-F**) Fluorescent images of a collagen matrix (CNA35-OG®488, green)) produced by osteoblasts and mineralized (Calcein Blue, magenta) in the presence of (**D**) mixed FetA/mineral complexes containing CPPs and CPMs, (**E**) isolated CPPs, or (**F**) βGP. Single channel images are available in Fig. S4A. We note lower intensity of the collagen signal in regions with a high mineral signal, due to the presence of the mineral limiting access of the collagen dye.

CPPs act as mineral source in osteoblast cell cultures

To examine whether these primary CPPs could contribute to bone matrix mineralization we exposed matrix-producing mouse osteoblast (MLO-A5) cultures (*14*) to biomimetic CPP-containing medium as well as to medium supplemented with isolated, preformed CPPs. In both cases, after 14 days of supplementation, fluorescence microscopy revealed matrix mineralization through the overlap of the mineral signal with the labeled collagen fibrils (Fig. 1D-E, Fig. S4A). The mineralization by the CPP-containing medium was qualitatively similar to that in standard osteogenic cell culture conditions using β-glycerophosphate (βGP) as phosphate source (Fig. 1F) where phosphate is generated by osteoblast-produced alkaline phosphatase (ALP). (*14-16*) CryoTEM also identified primary CPPs in the βGP supplemented culture medium (Fig. S1B), underlining that CPP formation in serum is directly linked to increased phosphate concentrations. No mineralization was observed in the absence of added calcium phosphate sources (calciprotein complexes/βGP, Fig. S1C).

Cell culture experiments with low FetA medium ([FetA]= 0.31mg/mL, Fig. S1D-E) using βGP as the mineral source, illustrated the role of FetA in regulating osteogenic matrix mineralization by controlling CaP precipitation. Here, we observed mineral deposition already after 7 days, compared to 14 days at

standard FetA concentration ([FetA]= 2.6 mg/mL, Fig. S1D-E), and with poor control over the mineralization process as evidenced by the formation of large globular precipitates, rather than homogeneous mineralization of the collagen matrix (Fig. S1F-H). No matrix mineralization was observed when CPPs were added to a cell culture where cellular activity was arrested by chemical fixation. This indicates that CPPs can serve as a mineral source during matrix mineralization, but only in the presence of active osteoblasts.

CPMs Mineralize Collagen, CPPs do Not

To further establish the role of osteoblast acivity in CPP-mediated matrix mineralization, we performed cell-free experiments in which we incubated bovine collagen type I fibrils with both freshly prepared and aged protein-mineral complex solutions, containing predominantly CPMs or only CPPs, respectively (Fig. S1A/S3, Table S1, Supplementary Text). CryoTEM revealed intrafibrillar mineralization of the collagen for the CPM solutions (Fig. 2A), in line with previous reports, (*17*) but no collagen mineralization was observed with the solutions containing only CPPs (Fig. 2B). Similarly no collagen mineralization was achieved with solutions suplemented with isolated mature CPPs, even after prolonged incubation (Fig. 2C). The above findings indicate that under the physiologically relevant conditions tested, only CPMs are able to directly deliver mineral to the collagen matrix, whereas CPPs require the involvement of the MLO-A5 cellular activity for their conversion into bioavailable CaP that can mineralize the collagen.

CPPs are Internalized and Processed via the Endo-Lysosomal Pathway

To understand how osteoblasts process CPPs, we fluorescently labeled both Fetuin-A and calcium in the protein-mineral complexes that were added to MLO-A5 cell cultures. 3D Airyscan microscopy showed dual-labeled CPPs within the intracellular space, consistent with active CPP internalization by osteoblasts (Fig. 2D-E), while no FetA or calcium signal was observed without addition of the CPPs (Fig. S4B). The CPP internalization was significantly reduced by the addition of methyl-beta-cyclodextrin (*18, 19*) (MβCD, ~3.6x, p=0.0005) or Dynasore (*20*) (~4.6x, p=0.0004), two well-known inhibitors of endocytosis, and abolished by incubation at low temperatures (4ºC, Fig. 2F-G, Fig. S4C-D).

Tracing the intracellular pathway of the fluorescently labeled CPPs by live imaging in the presence of Lysotracker® revealed the colocalization of FetA with acidic organelles (Pearson's coefficient: 0.7), (*21*) indicating lysosomal processing after endocytosis (Fig. 2H). Further tracing of the mineral was not possible due to the disintegration of the CPPs into their molecular and ionic components in the acidic medium of the lysosomes. Together, these results imply that bioavailability of the CPP mineral is achieved only after endocytic uptake and lysosomal processing by osteoblasts and we infer that this intracellular processing precedes the contribution to matrix mineralization.

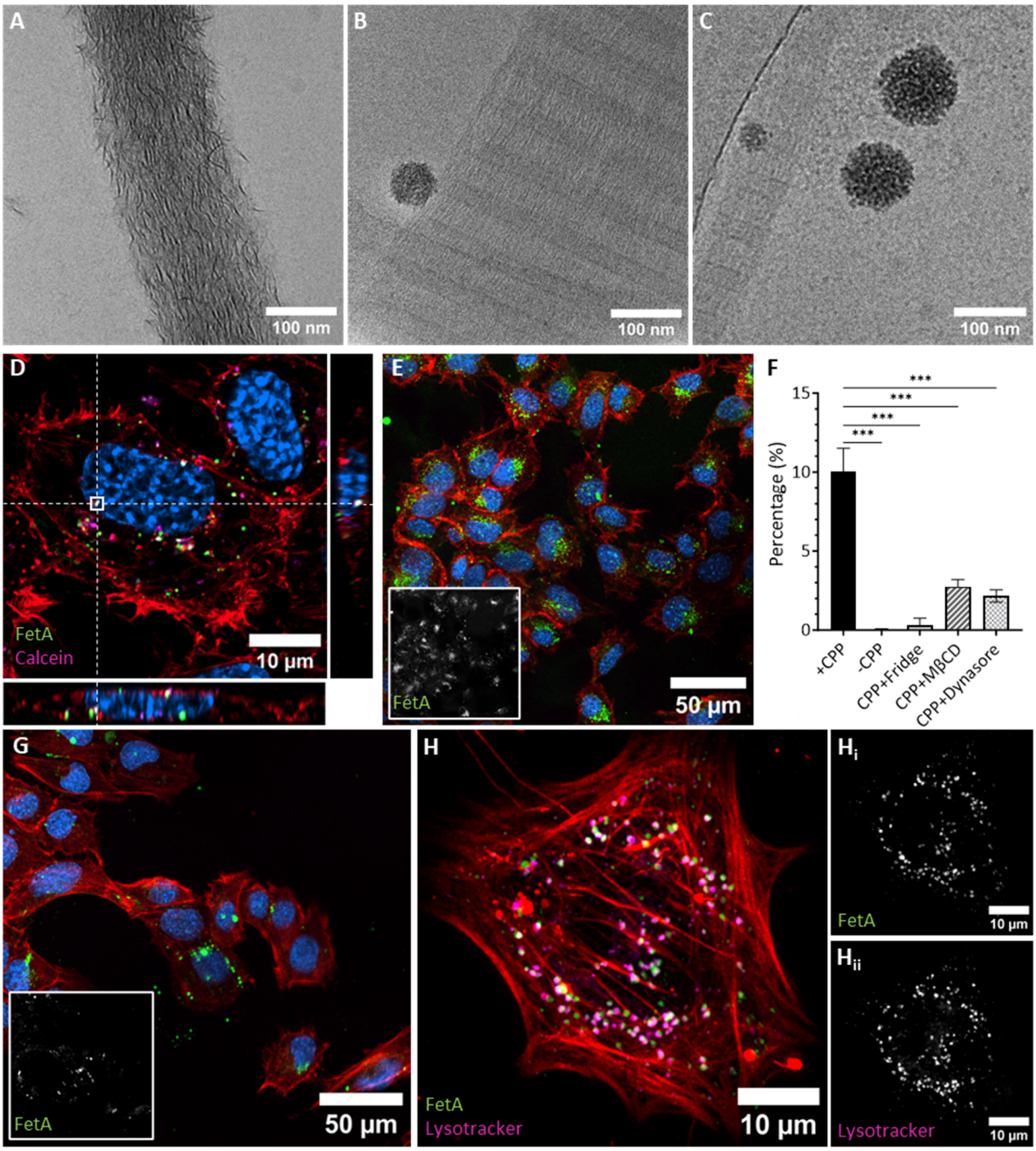

Fig. 2. Identification of two mineral delivery pathways by FetA/mineral complexes. (**A**) CryoTEM showed mineralized bovine collagen fibrils upon incubation (70 h, 37ºC) with freshly prepared biomimetic CPP formation medium, prepared from complete cell culture medium containing 10% FBS in αMEM supplemented with 3.0 mM phosphate. (**B**) Incubation (21 h, 37ºC) of bovine collagen fibrils with pre-formed mature FetA/mineral complexes (24 h incubated after addition of phosphate to CPP formation medium) showed no mineralization. (**C**) Prolonged incubation (70 h, 37ºC) of bovine collagen with concentrated, isolated mature CPPs (24 h old) did not result in collagen mineralization. (**D**) Orthogonal views of 3D fluorescence imaging show the presence of intracellular double labeled particles (FetA-CF®568, green; Calcein, magenta). (**E**) Fluorescent imaging of cells (actin: SiR-actin, red; nucleus: Hoechst 33342, blue) cultured in the presence of labeled FetA/mineral complexes (FetA-CF®568, green) showed FetA signal overlapping with cellular area. Inset: Isolated FetA channel. (**F**) Quantification of intracellular FetA signal in the presence and absence of CPPs, as well as in the presence of CPPs under endocytosis inhibiting conditions. Significance calculated by ANOVA multiple comparison analysis in GraphPad Prism (*** $p<0.001$). (**G**) Representative images showing MLO-A5 osteoblasts (actin: SiR-actin, red; nuclei: Hoechst 33342, blue) incubated with labeled in the presence of endocytosis inhibitor methyl-β-cyclodextrin. Inset shows the isolated FetA channel. Representative images of the other conditions can be found in Fig. S4. (**H**) MLO-A5 osteoblasts (actin:

SiR-actin, red) incubated with FetA-CF®568 labeled FetA/mineral complexes (green, **H_i**) and Lysotracker®-DND26 Green (magenta, **H_{ii}**) showing colocalization.

Dynamic assembly of Fetuin-A complexes explains functional differences

To resolve why CPMs but not CPPs directly mineralize collagen, we visualized the CPM-to-CPP transition using liquid-phase electron microscopy. Liquid phase electron microscopy (LP-EM) allows dynamic real-time visualization of CPP formation with nanoscale resolution, and at the electron dose applied here, without altering the kinetics of the assembly process. (*22*) Dynamic imaging of the biomimetic CPP formation medium within graphene-liquid cells (GLCs) showed the formation of small transient CPPs (tCPPs, diameters ~5-25 nm) by clustering of CPMs that assembled and disassembled dynamically (Fig. 3A-B, yellow arrows, Movie S1-S2, Fig. S5A). This dynamic process of continuous assembly and disassembly, was further illustrated by color-coding the FetA-mineral assemblies based on their size (Fig. 3A-B1, Movie S1-S2, Fig. S5B).

In contrast, larger CPPs (>50 nm) reached a stable size and no longer disassembled, neither did they show an increase in size after reaching a diameter of ~100 nm, suggesting they had matured to their maximum equilibrium size (Fig. 3B, blue arrows, Movie S2). Quantifying the size and the number of particles in the regions of interest over time (Fig. 3C, Fig. S5D) further showed the continuous (dis)assembly of tCPPs, however, changes in the size of a mature CPP were also observed. Structural dissimilarity index measure (DSSIM) analysis (*23*) further revealed internal dynamics within mature CPPs (Fig. 3D), with the constituting nanoparticulate subunits moving within the CPP perimeter (Fig. S5C). Moreover, and in line with previous reports, the prolonged incubation of the CPPs in the GLC for 14 days did lead to their transformation into secondary CPPs, as characterized by their oval shape, larger size (~350 nm long axis), and crystalline mineral content (Fig. S5E).

To understand this difference in dynamics between early stage and later stage assemblies we analysed the chemical composition of isolated CPMs and CPPs. This revealed that CPMs carried mineral complexes with a chemical composition (Ca:P ~0.4, Table S1) similar to previously reported pre-nucleation complexes ($[Ca(HPO_4)_3]^{4-}$ (*24*)). On the other hand, CPPs carried solid hydrated amorphous calcium phosphate (Ca:P ≈ 0.7), in agreement with the multi-stage development pathway of biomimetic CaP described by Habraken *et al.* (*24*). Furthermore, the Ca/protein ratios of the protein-mineral complexes were estimated to be 12 ± 2 for the CPMs and 16 ± 4 for the CCPs, respectively, impying that primary CPPs - formed at higher phosphate concentrations - are more efficient in transporting Ca than the CPMs. These findings suggest that maturation locks mineral into CPPs, preventing direct collagen mineralization but enabling storage and subsequent cell-mediated processing.

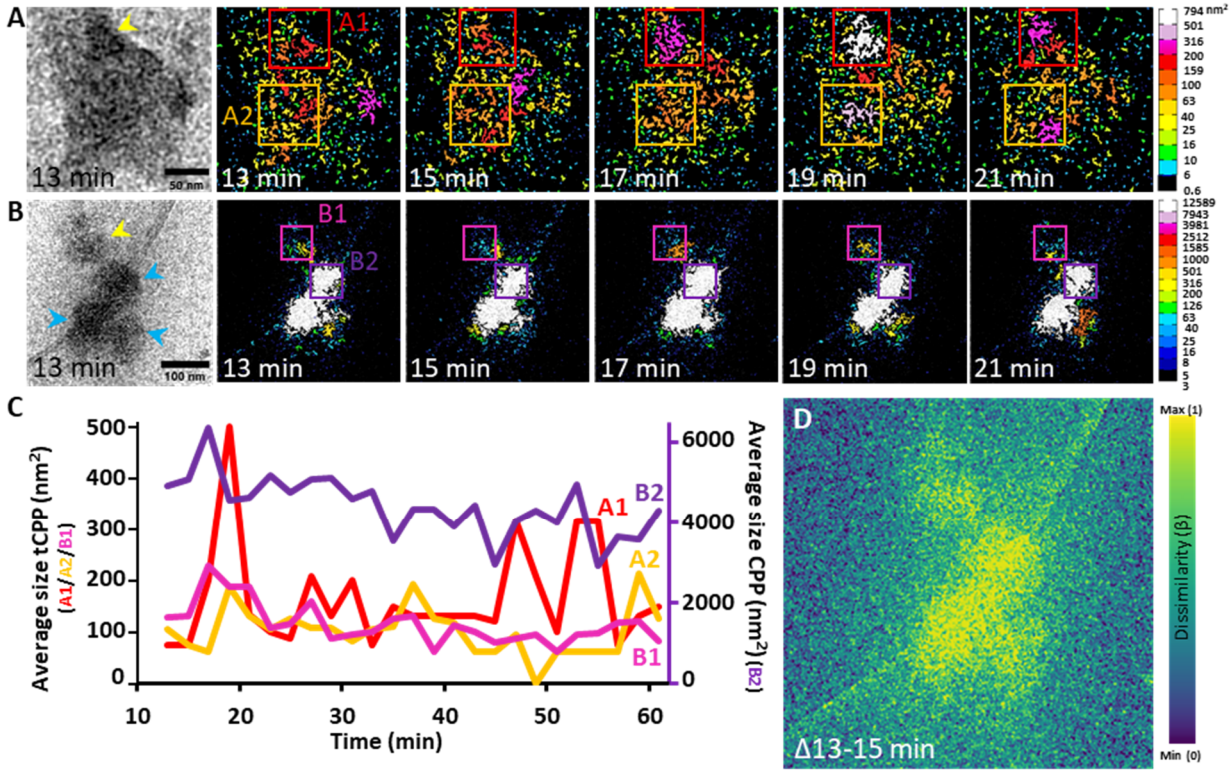

Fig. 3. Assembly of stable primary CPPs in cell culture medium is a two-phase process. (**A**) Dynamic monitoring of GLC with LP-EM, followed by color-based analysis of the particles based on the measured size (area, nm^2) of the particles showed the formation of small transient CPPs (<50 nm, tCPP, yellow arrow) by assembly and disassembly of CPM clusters (0.1 $e^- Å^{-2}$ per image), as indicated by region A1 and A2. The first image was recorded 13 min after addition of phosphate. Images were recorded every 2 minutes (Movie S1). Scalebar: 50 nm. (**B**) Time-lapse LP-EM and area-based color-coding (nm^2) of a GLC containing three mature primary CPPs (>50 nm, blue arrows, region B2) and an area in which tCPP (dis)assembly is observed (<50 nm, yellow arrow, region B1, Fig S3A). Scalebar: 100 nm. (**C**). Quantification of the particle size per region of interest (as indicated in (**A**) and (**B**)) during 62 minutes (images were recorded every 2 minutes). (**D**) Structural dissimilarity index measure (DSSIM) analysis of sequential frames in the recording of GLC (**B**) showed large changes within the particles, indicating intraparticle dynamics.

A Dual-Pathway Model for Fetuin-A–Mediated Mineral Delivery

Together, our experiments indicate two complementary pathways for FetA-dependent mineral transport from blood to bone. In the direct pericellular pathway, CPMs carrying dynamic pre-nucleation complexes deposit calcium phosphate into collagen fibrils without cellular involvement. In the indirect transcellular pathway, CPPs carrying solid hydrated ACP are endocytosed and processed by osteoblasts before their mineral becomes available for matrix mineralization. We propose that the direct CPM route supports routine bone remodeling, while the CPP-based pathway provides a high-capacity mineral supply during conditions of elevated systemic demand, such as fetal development, when when FetA, calcium and phosphate concentrations are elevated (*11, 12, 25, 26*), and the lifetime of CPPs may be longer due to the incomplete development of the liver. (*27*) Our conclusions are derived from serum-based osteoblast cultures; verification that these pathways are differentially engaged *in vivo* across developmental stages will require additional *ex vivo* and/or *in vivo* studies.

Acknowledgements:

The authors would like to thank Steffen Gräber from RWTH Aachen University Hospital for the purification of the Fetuin-A used for fluorescent labeling and FBS/medium supplementation. The authors also thank Thomas Kock and Gregory Schneider from Leiden University for supplying the graphene coated chips used in the LP-EM experiments.

Funding: JS, LR, ST, AS, MM, and NS were supported by a European Reseach Council (ERC) Advanced Investigator grant (H2020-ERC-2017-ADvV-788982-COLMIN). AA was supported by a VENI grant from the Netherlands Scientific Organization NWO (VI.Veni.192.094). EMS was supported by the Research Program Ramón y Cajal (RYC2023-045512-I) funded by MCIN/AEI/10.13039/501100011033 and FSE+, and the project PID2022-141993NA-I00 funded by MICIU/AEI/10.13039/501100011033 and ERDF/UE. WJD received funding from the Deutsche Forschungsgemeinschaft (DFG, German Research Foundation, Project-ID 322900939 and 403041552).

Author contributions:
Conceptualization: JS, LR, EMS, NS, AA
Methodology: JS, LR, ST, AS
Investigation: JS, LR, ST, AS, MM
Visualization: JS, LR, AA
Funding acquisition: EMS, WJD, NS, AA
Project administration: NS, AA
Supervision: JS, NS, AA
Writing – original draft: JS, NS, AA
Writing – review & editing: JS, LR, ST, AA, EMS, WJD, NS, AA

Competing interests:
Nothing to declare

References

1. A. Heiss *et al.*, Structural basis of calcification inhibition by alpha 2-HS glycoprotein/fetuin-A. Formation of colloidal calciprotein particles. *J. Biol. Chem.* **278**, 13333-13341 (2003).
2. A. Heiss, V. Pipich, W. Jahnen-Dechent, D. Schwahn, Fetuin-A is a mineral carrier protein: small angle neutron scattering provides new insight on Fetuin-A controlled calcification inhibition. *Biophys. J.* **99**, 3986-3995 (2010).
3. W. Jahnen-Dechent *et al.*, Mud in the blood: the role of protein-mineral complexes and extracellular vesicles in biomineralisation and calcification. *J. Struct. Biol.* **212**, 107577 (2020).
4. E. R. Smith, T. D. Hewitson, E. Hanssen, S. G. Holt, Biochemical transformation of calciprotein particles in uraemia. *Bone* **110**, 355-367 (2018).
5. E. R. Smith *et al.*, Phosphorylated fetuin-A-containing calciprotein particles are associated with aortic stiffness and a procalcific milieu in patients with pre-dialysis CKD. *Nephrology Dialysis Transplantation* **27**, 1957-1966 (2012).
6. P. Aghagolzadeh *et al.*, Calcification of vascular smooth muscle cells is induced by secondary calciprotein particles and enhanced by tumor necrosis factor-&#x3b1. *Atherosclerosis* **251**, 404-414 (2016).
7. S. Köppert *et al.*, Cellular Clearance and Biological Activity of Calciprotein Particles Depend on Their Maturation State and Crystallinity. *Front. Immunol.* **9**, 1991 (2018).
8. W. Jahnen-Dechent, A. Heiss, C. Schafer, M. Ketteler, Fetuin-A regulation of calcified matrix metabolism. *Circ. Res.* **108**, 1494-1509 (2011).
9. D. Toroian, P. A. Price, The essential role of fetuin in the serum-induced calcification of collagen. *Calcif. Tissue Int.* **82**, 116-126 (2008).
10. E. R. Smith, T. D. Hewitson, W. Jahnen-Dechent, Calciprotein particles: mineral behaving badly? *Curr. Opin. Nephrol. Hypertens.* **29**, 378-386 (2020).
11. M. Häusler, C. Schäfer, C. Osterwinter, W. Jahnen-Dechent, The Physiologic Development of Fetuin-A Serum Concentrations in Children. *Pediatric Research* **66**, 660-664 (2009).
12. W. Jahnen-Dechent, A. Pasch, Solving the insoluble: calciprotein particles mediate bulk mineral transport. *Kidney International* **103**, 663-665 (2023).
13. R. Gelli, F. Ridi, Reconsidering the role of albumin towards amorphous calcium phosphate-based calciprotein particles formation and stability from a physico-chemical perspective. *Colloids Surf. B. Biointerfaces* **227**, 113372 (2023).
14. Y. Kato *et al.*, Establishment of an Osteoid Preosteocyte-like Cell MLO-A5 That Spontaneously Mineralizes in Culture. *J. Bone Miner. Res.* **16**, (2001).
15. H. C. Tenenbaum, Role of Organic Phosphate in Mineralization of Bone in vitro. *J. Dent. Res.* **60**, 1586-1589 (1981).
16. J. M. Schaart *et al.*, Cell-induced collagen alignment in a 3D in vitro culture during extracellular matrix production. *J. Struct. Biol.* **216**, 108096 (2024).
17. F. Nudelman *et al.*, The role of collagen in bone apatite formation in the presence of hydroxyapatite nucleation inhibitors. *Nat. Mater.* **9**, 1004-1009 (2010).
18. J. J. Rennick, A. P. R. Johnston, R. G. Parton, Key principles and methods for studying the endocytosis of biological and nanoparticle therapeutics. *Nat. Nanotechnol.* **16**, 266-276 (2021).
19. D. Vercauteren *et al.*, The Use of Inhibitors to Study Endocytic Pathways of Gene Carriers: Optimization and Pitfalls. *Mol. Ther.* **18**, 561-569 (2010).
20. E. Macia *et al.*, Dynasore, a Cell-Permeable Inhibitor of Dynamin. *Dev. Cell* **10**, 839-850 (2006).
21. S. Bolte, F. P. Cordelières, A guided tour into subcellular colocalization analysis in light microscopy. *J Microsc*, (2006).
22. L. Rutten *et al.*, A Cryo-to-Liquid Phase Correlative Light Electron Microscopy Workflow for the Visualization of Biological Processes in Graphene Liquid Cells. *Adv. Funct. Mater.*, (2024).
23. J. T. Mulvey *et al.*, Correlating electrochemical stimulus to structural change in liquid electron microscopy videos using the structural dissimilarity metric. *Ultramicroscopy* **257**, 113894 (2024).
24. W. J. Habraken *et al.*, Ion-association complexes unite classical and non-classical theories for the biomimetic nucleation of calcium phosphate. *Nat Commun* **4**, 1507 (2013).
25. C. S. Kovacs, Bone metabolism in the fetus and neonate. *Pediatr. Nephrol.* **29**, 793-803 (2014).

26. C. S. Kovacs, Calcium, phosphorus, and bone metabolism in the fetus and newborn. *Early Hum. Dev.* **91**, 623-628 (2015).
27. J. Grijalva, K. Vakili, Neonatal liver physiology. *Semin. Pediatr. Surg.* **22**, 185-189 (2013).
28. J. Schindelin et al., Fiji: an open-source platform for biological-image analysis. Nat. Methods 9, 676-682 (2012).
29. K. N. Krahn, C. V. Bouten, S. van Tuijl, M. A. van Zandvoort, M. Merkx, Fluorescently labeled collagen binding proteins allow specific visualization of collagen in tissues and live cell culture. Anal. Biochem. 350, 177-185 (2006).
30. R. A. Boerboom et al., High resolution imaging of collagen organisation and synthesis using a versatile collagen specific probe. J. Struct. Biol. 159, 392-399 (2007).
31. C. H. Li, P. K. S. Tam, An iterative algorithm for minimum cross entropy thresholding. Pattern Recog. Lett. 19, 771-776 (1998).
32. J.-C. Yen, F.-J. Chang, S. Chang, A new criterion for automatic multilevel thresholding. IEEE Transactions on Image Processing 4, 370-378 (1995).
33. W. S. Rasband. (U. S. National Institutes of Health, Bethesda, Maryland, USA, 1997-2018).

Supplementary Materials

Materials and Methods

Supplementary Text

Figs. S1 to S5

Table S1

References (*28–33*)

Movies S1 to S3